OPEN ACCESS

International
Journal
Of Modern Engineering Research (IJMER)

Steady State and Faulty Behaviours of Solar Powered Three-Phase Induction Motor-Based Pumping System

Aarinola G Akinseloyin[1], Oluwole S.A[2], Oricha, J.Y[3], Orogun O, Emmanuel[4]
Ogundipe R, Josiah[5],Ojo O, David[6]
[1,2]*Department of Electrical & Electronics Engineering, Faculty of Engineering, Federal University, Oye-Ekiti, Nigeria*

ABSTRACT
This research investigates the dynamic characteristics and fault response patterns of a solar-powered three-phase induction motor system across varying operational conditions. A comprehensive simulation study was conducted examining three key aspects: steady-state performance, environmental influence, and fault scenarios. The steady-state analysis revealed stable system behaviour with balanced three-phase output and consistent motor operation. Environmental impact assessment demonstrated significant correlation between solar irradiance variations and system performance metrics. The fault analysis explored three critical scenarios: AC open circuit faults, three-phase to ground faults, and phase-to-phase faults. Results indicated that three-phase to ground faults posed the most severe threat to system integrity, characterised by voltage collapse and extreme current surges, while phase-to-phase faults exhibited moderate impact through waveform distortion and unbalanced current flow. Steady-state testing confirmed robust performance under normal conditions, with stable DC input voltage, balanced AC output, and consistent rotor speed. These findings provide valuable insights for developing enhanced protection mechanisms and control strategies for PV-powered motor systems, contributing to the advancement of reliable renewable energy solutions. The research outcomes offer practical recommendations for implementing more effective fault detection and protection schemes in similar applications.

Date of Submission: 15-06-2025 Date of acceptance: 30-06-2025

I. INTRODUCTION

The increasing demand for renewable energy sources has catalysed significant interest in solar-powered systems, particularly in water pumping applications. Solar-powered pumping systems present notable advantages over conventional fossil fuel-based alternatives, including reduced operational costs, enhanced environmental sustainability, and independence from the electrical grid (Renu et al., 2013). Among these systems, the configuration incorporating a three-phase induction motor coupled with a photovoltaic (PV) array, boost converter, and power inverter has emerged as a prominent solution.

Three-phase induction motors have established themselves as the cornerstone of industrial applications, owing to their inherent robustness, reliability, and minimal maintenance requirements (Pillay & Krishnan, 1989). However, their operational efficiency is susceptible to various factors, including supply voltage imbalances, harmonic distortions, and component faults. These challenges can manifest in increased power losses, diminished system efficiency, and potential motor degradation (Abdelrahman et al., 2020). The integration of photovoltaic arrays, whilst offering the advantage of direct solar energy conversion, introduces additional complexities due to output voltage variations influenced by environmental conditions such as temperature and solar irradiance (Villalva et al., 2009; Arulkumaran et al., 2015).

The contemporary landscape of single-phase transformerless grid-connected PV systems presents unique challenges in fault detection and classification. Traditional fault detection methodologies often prove inadequate when confronted with the intricacies of transformerless topologies, where the absence of galvanic isolation heightens system vulnerability to specific fault types (Arafa et al., 2017; Raghuwanshi and Gupta, 2015). Conventional threshold-based detection approaches frequently result in false alarms or missed detections, primarily due to the dynamic nature of PV system operations and fluctuating environmental conditions (Khan et al., 2022; Ahmad et al., 2018).

Whilst numerous studies have investigated various aspects of solar-powered three-phase induction motor systems, several critical limitations persist in existing research. Studies focusing on PV array optimisation, such as those by Kurukuru et al. (2016), have often overlooked the arrays' impact on overall system efficiency. Research concerning boost converters, like that of Bharadwaj & Sanjeevikumar (2017), has predominantly concentrated on standalone performance metrics, neglecting the dynamic nature of PV input. Similarly, investigations into power inverters, such as Khawaldah et al. (2021), have frequently disregarded the specific requirements of three-phase induction motors in pumping applications. Moreover, studies examining three-phase induction motors, including Abdelrahman et al. (2020), have typically emphasised grid-connected systems, failing to address the unique challenges presented by solar power integration.

Recent advances in machine learning have demonstrated promise in fault detection applications. However, there remains a critical need for comprehensive comparative analysis of different classification algorithms specifically tailored for transformerless PV systems utilising wavelet-based feature extraction (Chen et al., 2022; Wang et al., 2024; Rodriguez et al., 2024). The integration of wavelet transform with multiple machine learning approaches for optimal fault classification accuracy, whilst maintaining effective fault discrimination capabilities for component-level faults, represents a significant research gap (Kibria et al., 2023; Barkat et al., 2023).

This research aims to critically investigate the steady-state and faulty behaviours of a solar-powered three-phase induction motor based pumping system. The investigation encompasses several key objectives: developing and integrating accurate mathematical models for the system components, analysing system behaviour under varying environmental and operational conditions, simulating diverse fault scenarios to understand their impact on system performance, and validating the developed model through comparison with existing literature and theoretical predictions. This comprehensive approach addresses the identified research gaps whilst contributing to the advancement of sustainable energy systems.

2.1 Empirical Review

Yilmaz and Martínez-Morales (2023) investigated fault detection in photovoltaic panels using Digital Twin technology. Their methodology involved creating a digital replica of the PV system to enable real-time fault simulation and prediction. The study demonstrated that Digital Twin technology significantly improved fault detection accuracy compared to conventional methods by enabling predictive maintenance capabilities. However, the research was limited by the high computational requirements and complexity of implementing Digital Twin models, making it potentially impractical for simpler transformerless PV systems.

Kim (2023) developed a PV junction box monitoring system utilizing LoRa technology for real-time fault detection. The study implemented LoRa-based sensors to monitor system performance parameters and wirelessly transmit fault data. The results showed successful fault detection with stable performance and energy-efficient operation. The main limitation was the system's dependence on wireless connectivity, which could compromise fault detection reliability in areas with poor signal coverage.

Lahiouel et al. (2023) presented an adaptive neuro-fuzzy inference system (ANFIS) for fault detection in photovoltaic systems. Their methodology combined neural networks with fuzzy logic principles to classify various fault types under different operating conditions. The results indicated high detection accuracy and reduced maintenance costs. However, the system's performance was heavily dependent on training data quality and struggled with real-time applications in rapidly changing environmental conditions.

Sakthivel et al. (2023) explored fault detection, classification, and location in solar PV arrays using a single sensor approach. Their methodology focused on analysing voltage signals to identify and classify open-circuit and short-circuit faults. While the approach proved cost-effective and widely applicable, its reliance on a single sensor limited fault localization accuracy in complex transformerless PV systems.

Ahir et al. (2024) developed an informed change-point detection approach for identifying unauthorized solar PV installations in smart grids. Their methodology employed statistical techniques to detect anomalies in electricity consumption patterns, achieving an F1-score of 97%. However, the study didn't address fault detection in transformerless PV systems or explore wavelet-based and machine learning techniques for fault classification.

Jafariazad et al. (2024) proposed an adaptive supplementary control system for virtual synchronous generators in grid-connected and islanded microgrids. Their methodology utilized adaptive virtual impedance to minimize voltage tracking errors and limit fault currents. While the study showed improved fault response, it focused primarily on microgrids rather than transformerless PV systems.

Xia et al. (2021) developed a comprehensive MATLAB/Simulink model for a solar-powered three-phase induction motor pumping system. Their methodology included detailed modelling of the PV array, boost converter, three-phase inverter, and induction motor, with analysis of various fault conditions. While the model was comprehensive, it didn't address economic considerations in system design.

Bouzidi et al. (2022) focused on optimizing solar-powered water pumping systems using genetic algorithms. Their methodology incorporated mathematical modelling of system components and employed genetic algorithms to optimize design parameters for cost minimization. The study's limitation was its primary focus on cost optimization without fully addressing system reliability and performance under various operating conditions.

Sayed et al. (2022) developed a machine learning-based fault diagnosis technique for PV arrays. Their methodology demonstrated high accuracy in detecting and classifying various fault types. However, the study was limited to PV array faults and didn't address issues in other system components.

Khawaldah et al. (2021) proposed an advanced inverter control strategy for three-phase grid-connected PV systems using model predictive control. While their approach improved power quality and system efficiency, it was specifically designed for grid-connected systems and may not be directly applicable to standalone operations.

The literature review reveals several significant gaps in existing research. First, most studies focus on individual components rather than taking a holistic system approach. Second, there's limited research on fault detection and classification in standalone solar-powered TPIM pumping systems, particularly regarding the integration of advanced techniques like machine learning and wavelet analysis. Third, existing models often fail to consider the dynamic interaction between system components under both steady-state and fault conditions.

The current research aims to address these gaps by developing a comprehensive model that integrates detailed component modelling with advanced fault detection and classification techniques. This approach will provide deeper insights into system behaviour under various operating conditions and fault scenarios, leading to improved design and operational strategies for solar-powered TPIM pumping systems.

II. RESEARCH METHODOLOGY

3.1 Mathematical Model of Solar PV

The equivalent circuit of a solar cell is shown in Figure 1.

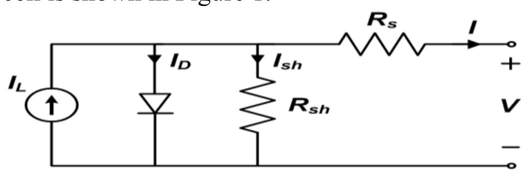

Figure 1: Single-Diode Equivalent Circuit Model

The current-voltage (I-V) characteristic equation of the solar cell can be expressed as:

$$I = I_{ph} - I_o\left[\exp\left(\frac{V + IR_s}{a \times V_t}\right) - 1\right] - \frac{V + IR_s}{R_{sh}} \quad (1)$$

Where:
I is the cell output current (A)
V is the cell output voltage (V)
I_{ph} is the photocurrent or light-generated current (A)
I_o is the reverse saturation current of the diode (A)
R_s is the series resistance (Ω)
R_{sh} is the shunt resistance (Ω)
a is the diode ideality factor (dimensionless)
V_t is the thermal voltage (V)

The photocurrent I_{ph} depends on the solar irradiance and cell temperature and can be expressed as:

$$I_{ph} = [I_{sc} + K_i(T_c - T_r)] \times \left(\frac{G}{G_r}\right) \quad (2)$$

Where:
I_{sc} is the short-circuit current at reference conditions (A)
K_i is the short-circuit current temperature coefficient (A/°C)
T_c is the cell operating temperature (°C)
T_r is the reference temperature (°C)
G is the actual solar irradiance (W/m²)

G_r is the reference solar irradiance (W/m²)
The reverse saturation current Io is given by:

$$I_o = I_{ors} \times \left(\frac{T_c}{T_r}\right)^3 \times \exp\left[\frac{\left(E_g \times q\right)}{(a \times k)} \times \left(\frac{1}{Tr} - \frac{1}{Tc}\right)\right] \quad (3)$$

Where:
I_{ors} is the reverse saturation current at reference conditions (A)
E_g is the bandgap energy of the semiconductor (eV)
q is the electron charge $(1.602\ x\ 10^{-19} C)$
k is the Boltzmann constant $\left(1.381\ x \frac{10^{-23} J}{K}\right)$
The thermal voltage V_t is defined as:

$$V_t = \frac{a \times k \times Tc}{q} \quad (4)$$

The parameters $I_{sc}, V_{oc}, K_i, I_{ors}, R_s, R_{sh}$, and a are typically provided by the manufacturer or can be determined through experimental measurements and curve-fitting techniques.
The PV array was modelled using the parameters provided in Table 1, which specifies the characteristics of the photovoltaic module at standard test conditions (STC) with an irradiance of $1000 w/m^2$ and a temperature of 25°C. To achieve the desired input voltage of 377V for the VSI, a total of 10 panels were connected in series.
For this design, the maximum power (P) of the MPPT was designed for 3200W. The MPPT controller will be designed to provide the maximum current (I_{mppt}) from the PV array, calculated as:

$$I_{mppt} = \frac{P}{V} = \frac{3200}{377} = 8.5A \quad (5)$$

The VSI coupling capacitor (C) will be determined using the following equation:

$$C = \frac{I_{mppt}}{F_S \times V} = \frac{8.5}{10000 \times 377} = 2.25uf \quad (6)$$

Where F_S is the switching frequency of the VSI, and V is the input voltage (377V).
The VSI was modelled to convert the DC input voltage from the PV array into a three-phase AC voltage to drive the TPIM.

Table 1: Characteristics of Photovoltaic module at STC (G = 1000 W/m^2 and T = 25 °C)

Parameters	**Values**
Maximum Power (Pmax)	320W
Maximum Voltage (Vmpp)	37.7V
Maximum current (Impp)	8.41 A
Short circuit current (Isc)	8.98 A
Open circuit Voltage (Voc)	46 V

3.3 Mathematical Model of MPPT Charge Controller

The MPPT charge controller in the solar water pumping system is responsible for regulating the output voltage of the solar PV array and providing the appropriate voltage level to the boost converter.
The MPPT charge controller can be modelled as a voltage source with a variable output voltage (V_{MPPT}) that is dependent on the solar irradiance level and temperature. The output voltage V_{MPPT} can be expressed as a function of the open-circuit voltage (Voc) of the solar PV array:

$$V_{MPPT} = k \times V_{oc} \quad (7)$$

Where k is a constant factor, typically in the range of 0.7 to 0.8, representing the approximate voltage at which the PV array operates at its maximum power point.
The open-circuit voltage V_{oc} of the solar PV array can be modelled using the single-diode equivalent circuit model, as described in Section 3.2. V_{oc} is the voltage across the solar cell when no current is flowing, and it can be expressed as:

$$V_{oc} = (a * V_t) \times \ln\left(\frac{\left(I_{ph} + I_o\right)}{I_o}\right) + \left(I_{ph} \times R_s\right) \quad (8)$$

Where:
V_t is the thermal voltage (V)
a is the diode ideality factor (dimensionless)
I_{ph} is the photocurrent or light-generated current (A)
I_o is the reverse saturation current of the diode (A)
R_s is the series resistance (Ω)
The photocurrent I_{ph} and the reverse saturation current I_o are dependent on the solar irradiance level and temperature, as discussed in Section 3.2.
This simplified approach allows the integration of the MPPT charge controller model into the overall system model, enabling the analysis of steady-state and faulty behaviours of the solar-powered three-phase induction motor-based pumping system, as per the research objectives.

3.4 Mathematical Model of Voltage Source Inverter (VSI)

The voltage source inverter (VSI) is a crucial component in the solar water pumping system, as it converts the DC voltage from the boost converter into a three-phase AC voltage to drive the three-phase induction motor (TPIM). The mathematical model of the VSI is essential for analysing the system's behaviour and performance.
The VSI consists of six power switches (typically IGBTs or MOSFETs) arranged in a bridge configuration, as shown in Figure 2.

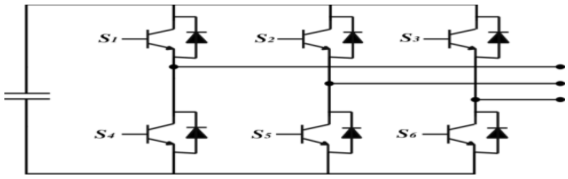

Figure 2: Three-phase voltage source inverter (VSI) configuration

The switches operate in a complementary manner, where the switches in the same leg (e.g., S_1 and S_4) are never turned on simultaneously to avoid short-circuiting the DC link.
The mathematical model of the VSI can be derived by analysing the switching states and applying Kirchhoff's voltage and current laws. The output voltages of the VSI ($V_{AN}, V_{BN}, and\ V_{CN}$) can be expressed in terms of the switching states and the DC link voltage (V_{dc}):

$$V_{AN} = \left(\frac{2}{3}\right) \times \left(S_a - \left(\frac{1}{2}\right) \times (S_b + S_c)\right) \times V_{dc} \quad (3.7)$$

$$V_{BN} = \left(\frac{2}{3}\right) \times \left(-S_a + S_b - \left(\frac{1}{2}\right) \times S_c\right) \times V_{dc} \quad (3.8)$$

$$V_{CN} = \left(\frac{2}{3}\right) \times \left(-S_a - S_b + \left(\frac{1}{2}\right) \times S_c\right) \times V_{dc} \quad (3.9)$$

Where:
$S_a, S_b, and\ S_c$ are the switching states of the three legs (0 or 1)
Vdc is the DC link voltage from the boost converter
The output currents of the VSI ($i_a, i_b, and\ i_c$) can be determined by applying Kirchhoff's current law to the three-phase load (TPIM):

$$i_a + i_b + i_c = 0 \quad (3.10)$$

The mathematical model of the VSI can be integrated with the models of the TPIM and other system components to analyse the overall system behaviour and performance.

3.5 Mathematical Model of Three-Phase Induction Motor (TPIM)

The three-phase induction motor (TPIM) is the prime mover in the solar water pumping system, converting the electrical energy from the voltage source inverter (VSI) into mechanical energy to drive the pump. The mathematical model of the TPIM can be derived from the basic principles of electromagnetic theory and the equivalent circuit representation of the motor. The model can be developed in either the stationary reference frame (α-β frame) or the synchronously rotating reference frame (d-q frame). In this research, the model is presented in the synchronously rotating d-q reference frame, which simplifies the analysis by eliminating time-varying inductances. The simplified equivalent circuit of three-phase induction motor is shown in Figure 3 where Figure 3(a) is the q-frame referenced equivalent circuit while Figure 3(b) is the d-frame referenced equivalent circuit.

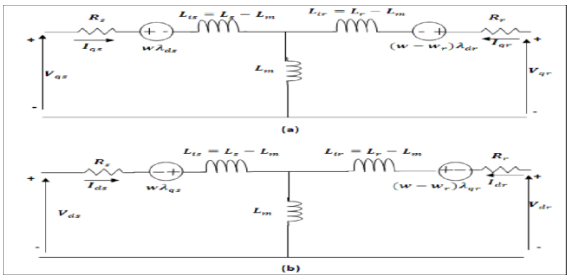

Figure3: Simplified equivalent circuit of TPIM (Koh *et al*., 2023)

The voltage equations of the TPIM in the d-q reference frame can be expressed as:

$$V_{qs} = (R_s \times i_{qs}) + \left(\frac{d\lambda_{qs}}{dt}\right) + (\omega_r \times \lambda d_s) \quad (9)$$

$$V_{ds} = (R_s \times i_{ds}) + \left(\frac{d\lambda_{ds}}{dt}\right) - (\omega_r \times \lambda_{qs}) \quad (10)$$

$$V_{qr} = (R_r \times i_{qr}) + \left(\frac{d\lambda qr}{dt}\right) + (\omega_r - \omega_m) \times \lambda_{dr} \quad (11)$$

$$Vdr = (R_r \times i_{dr}) + \left(\frac{d\lambda dr}{dt}\right) - \left((\omega_r - \omega_m) \times \lambda qr\right) \quad (12)$$

Where:
$V_{qs}, V_{ds}, V_{qr}, and\ V_d$r are the stator and rotor voltages in the d-q frame
$i_{qs}, i_{ds}, i_{qr}, and\ i_{dr}$ are the stator and rotor currents in the d-q frame
$\Lambda_{qs}, \lambda_{ds}, \lambda_{qr}, and\ \lambda_{dr}$ are the stator and rotor flux linkages in the d-q frame
$R_s and\ R_r$ are the stator and rotor resistances
ω_r is the electrical angular speed of the rotating reference frame
ω_m is the mechanical angular speed of the rotor
The flux linkages are related to the currents and inductances as follows:

$\lambda_{qs} = L_{ls} \times i_{qs} + L_m \times (i_{qs} + i_{qr})$ (13)
$\lambda_{ds} = L_{ls} \times i_{ds} + L_m \times (i_{ds} + i_{dr})$ (14)
$\lambda_{qr} = L_{lr} \times i_{qr} + L_m \times (i_{qs} + i_{qr})$ (15)
$\lambda_{dr} = L_{lr} \times i_{dr} + L_m \times (i_{ds} + i_{dr})$ (16)

Where:
$L_{ls} and\ L_{lr}$ are the stator and rotor leakage inductances
L_m is the mutual inductance between the stator and rotor windings
The electromagnetic torque developed by the TPIM can be expressed as:

$$T_e = \left(\frac{3}{2}\right) x \left(\frac{P}{2}\right) \times (\lambda_{ds} \times i_{qs} - \lambda_{qs} \times i_{ds}) \quad (17)$$

Where P is the number of pole pairs.
The mechanical equation of motion for the TPIM is given by:

$$J\left(\frac{d\omega_m}{dt}\right) + B \times \omega_m = T_e - T_L \quad (18)$$

Where:
J is the combined inertia of the motor and the load
B is the combined viscous friction coefficient
T_L is the load torque (the pump torque in the water pumping system)
The TPIM was modelled based on the specifications presented in Table 2. The motor has a rated power of 2.5 kW, a rated voltage of 380V, and a rated speed of 1880 rpm. It was configured with four poles and a star-connected winding arrangement.

Table1: Specifications of the 3-phase IM

Parameters	**Values**
Rated power	2.5 kw
Rated voltage	380V
Rated speed	1880 (rpm)

No. of poles	4
Winding	Star connected
Resistance	R1 = 1.115 Ω
	R2 = 1.083 Ω
Inductance	X1= X2 = 5.974 (mH)
	Xm = 203.7 (mH)

The overall MATLAB/Simulink modelintegrated the PV array, MPPT controller, VSI, TPIM, and the pump. This model will enable the analysis of the system's performance under various operating conditions, such as varying solar irradiance levels and pumping loads.

4.1 Results

4.1.1 Steady State Analysis

The steady-state characteristics of the system under normal operating conditions are presented in Figure 4, which displays four critical parameters. The DC input voltage from the PV array exhibits stable behaviour with minimal fluctuation during steady-state operation. The three-phase AC voltage output from the inverter demonstrates a well-balanced sinusoidal waveform across all phases. Similarly, the three-phase AC current flowing through the induction motor maintains a balanced sinusoidal pattern. The rotor speed settles at a constant value once steady-state conditions are achieved.

Analysis of these steady-state characteristics reveals robust system performance under normal operating conditions. The balanced nature of both voltage and current waveforms indicates proper power conversion from DC to AC through the inverter. The stable rotor speed suggests effective electromechanical energy conversion within the induction motor, with minimal electromagnetic torque ripple. This stability is crucial for the longevity of the motor and the overall reliability of the system.

4.1.2 Solar Irradiance Impact

The system's response to environmental variations, particularly solar irradiance and temperature changes, is documented in Figure 5. The results show distinct variations in system parameters corresponding to changes in solar irradiance levels.

Analysis of these characteristics reveals the system's sensitivity to environmental conditions. The relationship between solar irradiance and system performance parameters demonstrates the direct impact of environmental factors on power generation capability. This understanding is crucial for predicting system behaviour under varying weather conditions and implementing appropriate control strategies to maintain optimal performance.

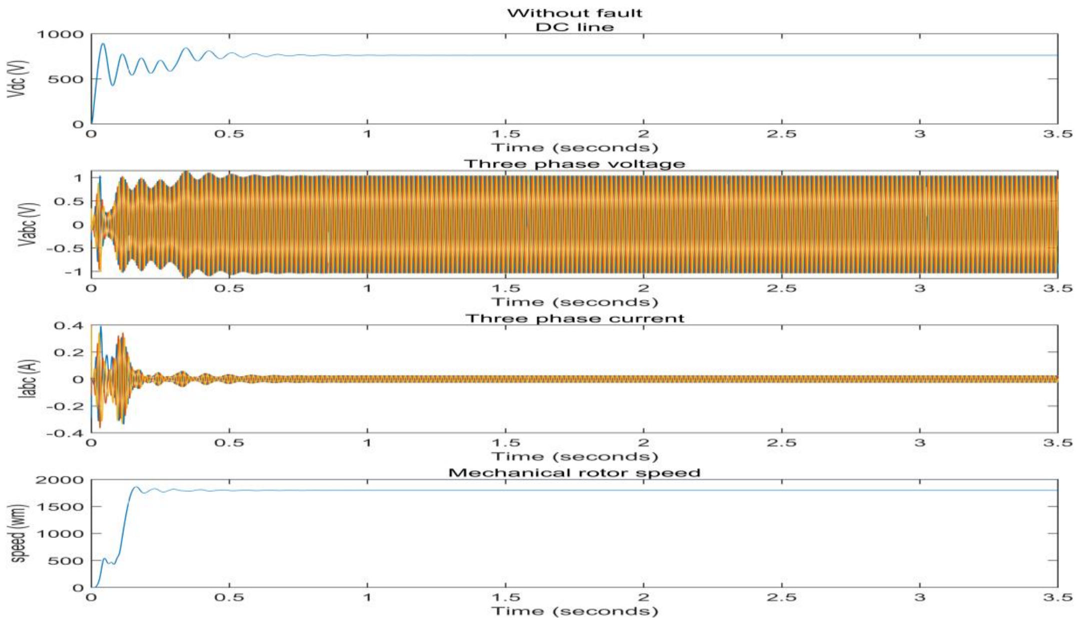

Figure 4: Steady State Characteristics at no faults for DC Input Voltage, Three Phase AC Voltage, Three Phase AC current and Rotor Speed

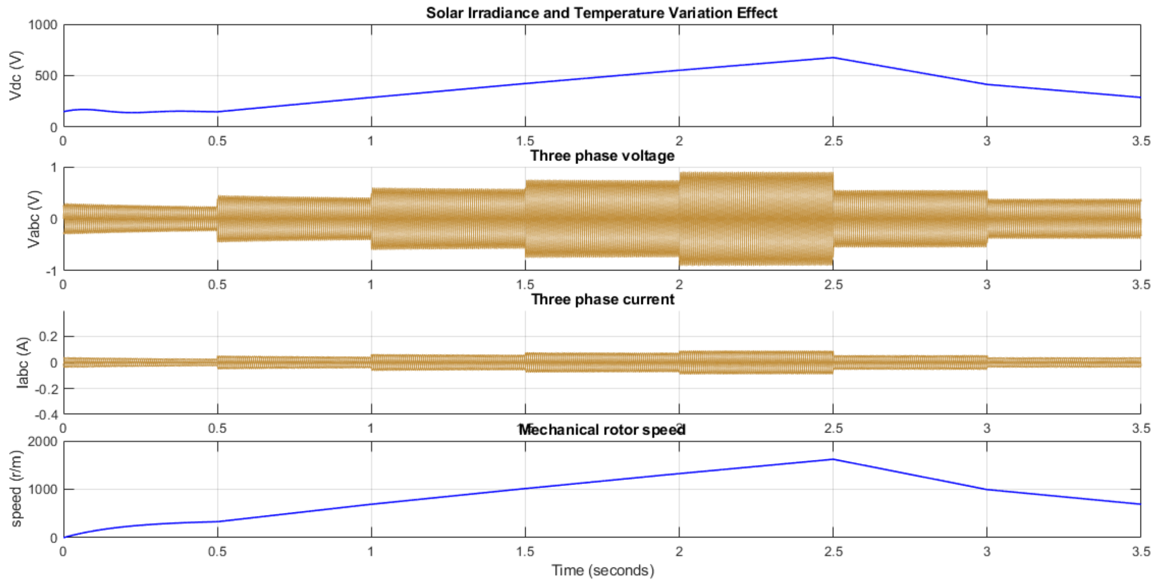

Figure 5: System Characteristics under Varying Solar Irradiance

4.1.3 Fault Scenarios Analysis

Three distinct fault scenarios were investigated, as presented in Figures 6, 7, and 8. The AC open circuit fault results, shown in Figure 6, demonstrate significant disturbances in system parameters, including disruption of the DC link voltage, interruption of three-phase AC voltage and current, and consequent effects on rotor speed. The three-phase to ground fault results, illustrated in Figure 7, reveal more severe system impacts, including DC voltage fluctuations, complete collapse of three-phase voltage, substantial current surges, and rapid motor deceleration. The phase-to-phase fault characteristics, presented in Figure 8, show intermediate severity with notable distortions in voltage waveforms and unbalanced current flow.

Analysis of these fault scenarios indicates varying degrees of system stress and potential damage risks. The AC open circuit fault demonstrates the system's vulnerability to supply interruptions, while the three-phase to ground fault represents the most severe condition, capable of causing significant damage to system components. The phase-to-phase fault results suggest moderate system stress with particular impact on motor performance due to electrical unbalance.

4.2 Discussion of Findings

The comprehensive analysis of steady-state operation, environmental impacts, and fault scenarios reveals several significant findings about the system's behaviour and resilience. The steady-state results demonstrate the system's capability to maintain stable operation under normal conditions, with well-regulated voltage and current profiles supporting consistent motor performance. The solar irradiance study highlights the system's dependence on environmental conditions, emphasising the need for robust control strategies to manage power fluctuations.

The fault analysis results are particularly noteworthy, revealing a hierarchy of fault severity and system vulnerability. The three-phase to ground fault emerges as the most critical condition, requiring immediate protective action to prevent system damage. The phase-to-phase and AC open circuit faults, while less severe, still present significant risks to system integrity and motor performance. These findings underscore the importance of implementing comprehensive protection schemes and fault detection mechanisms to ensure system reliability and longevity.

The overall results suggest that while the system demonstrates robust performance under normal conditions, it requires carefully designed protection mechanisms to guard against various fault scenarios. Future development should focus on enhancing fault tolerance and implementing more sophisticated control strategies to maintain stable operation under varying environmental conditions.

V. CONCLUSION AND RECOMMENDATIONS

5.1 Conclusion

This research has provided valuable insights into the behaviour and performance of a PV-powered three-phase induction motor system under various operating conditions. The steady-state analysis demonstrated the system's capability to maintain stable operation with balanced three-phase output and consistent motor performance. The investigation of environmental impacts revealed the significant influence of solar irradiance on system performance, highlighting the need for robust control strategies. The fault analysis uncovered varying degrees of system vulnerability, with three-phase to ground faults posing the most severe threat to system integrity. Through comprehensive analysis of normal operation and fault scenarios, this study has established a foundation for improving the reliability and resilience of PV-powered motor systems in practical applications.

5.2 Recommendations

The following recommendations are proposed based on the research findings:

i. Development and integration of sophisticated protection mechanisms specifically designed to detect and respond to three-phase to ground faults, as these were identified as the most severe fault condition.

ii. Installation of comprehensive environmental monitoring systems to track solar irradiance and temperature variations in real-time. This will enable better prediction of system performance and allow for proactive adjustments to maintain optimal operation under varying conditions.

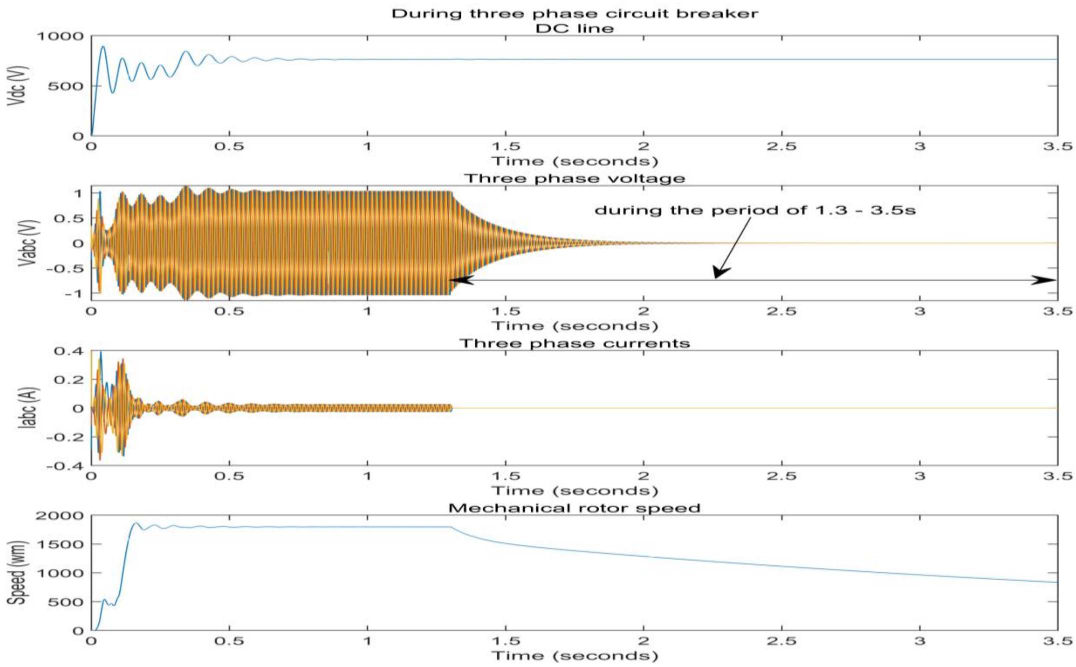

Figure 6: AC Open Circuit (AC Circuit Breaker Open) Fault Transient Characteristics for DC Voltage, Three-Phase AC Voltage, Three-Phase AC Current and Three-Phase Rotor Speed

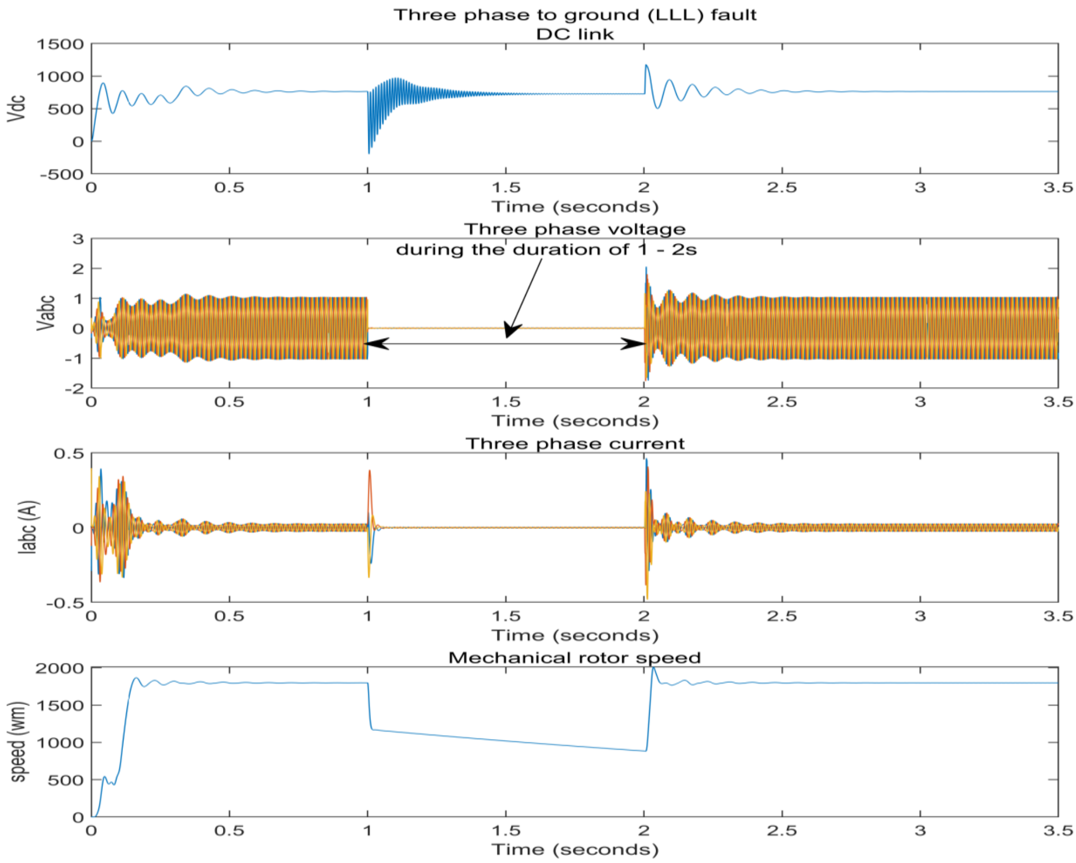

Figure 7: Three Phase to Ground (L-L-L-G) Fault Transient Characteristics for DC Voltage, Three-Phase AC Voltage, Three-Phase AC Current and Three-Phase Rotor Speed

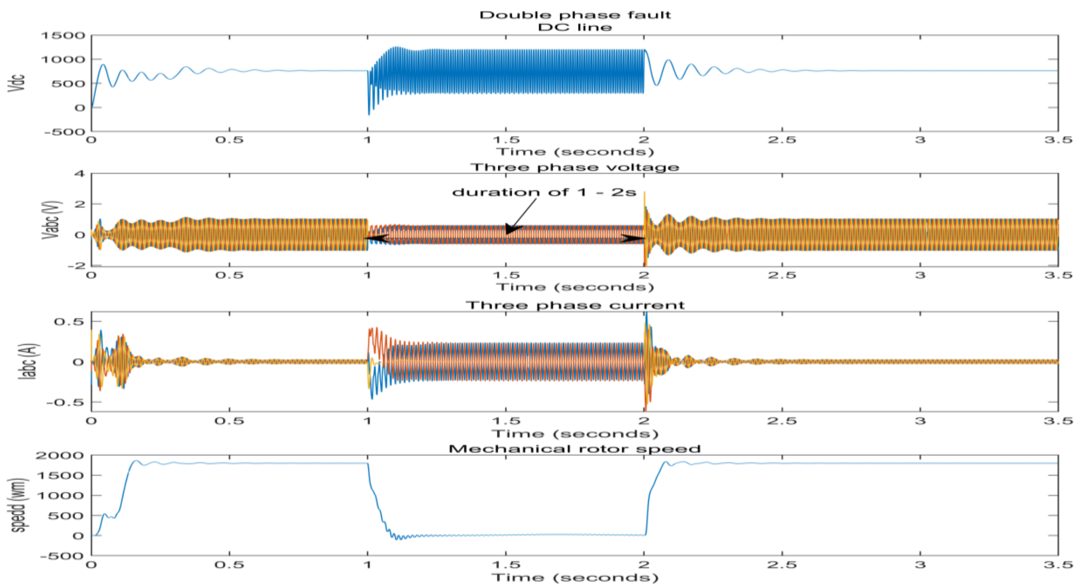

Figure 8: Phase to Phase (L-L) Fault Transient Characteristics for DC Voltage, Three-Phase AC Voltage, Three-Phase AC Current and Three-Phase Rotor Speed

iii. Design and implement advanced control strategies that can maintain system stability during minor faults and ensure graceful degradation during severe fault conditions

iv. Establish a systematic approach to monitoring key system parameters and implementing predictive maintenance protocols.

5.3 Research Limitations

The research conducted faced several limitations that should be acknowledged for future investigations. The simulation-based approach, while comprehensive, may not fully capture all real-world conditions and system interactions that could affect performance. The environmental impact analysis was limited to solar irradiance and temperature variations, while other environmental factors such as humidity and dust accumulation were not considered. Additionally, the fault analysis focused on specific fault types, while other potential failure modes and their combinations were not investigated. The time constraints of the study also limited the exploration of long-term degradation effects and the impact of repeated fault conditions on system components.

5.4 Conflict of Interest

The authors declare no conflict of interest in the conduct and reporting of this research. All funding sources and support have been properly acknowledged, and no commercial or financial relationships that could be construed as a potential conflict of interest existed during the course of this study. The research was conducted with complete academic independence, and all results have been reported without bias or external influence.

REFERENCES

[1]. Abdelrahman, A. S., Youssef, A., & Abou-Hashim, M. (2020). A review on faulty behaviour of three-phase induction motors. *IEEE Access, 8*, 116965–116975. https://doi.org/10.1109/ACCESS.2020.3004571

[2]. Arafa, A. M., Sayed, M. A., & Hassan, R. A. (2017). Fault detection in transformerless photovoltaic systems. *IEEE Transactions on Energy Conversion*.

[3]. Arulkumaran, S., Vijayakumar, D., & Nachiar, C. K. (2015). A new maximum power point tracking converter for solar-powered DC motor drive applications. *International Journal of Photoenergy, 2015*, 1–8. https://doi.org/10.1155/2015/610980

[4]. Barkat, A., Kibria, A. N. M., & Ahmed, S. A. (2023). Comparative analysis of wavelet-based and machine learning fault classification methods. *Journal of Solar Energy Research*.

[5]. Bharadwaj, A., & Sanjeevikumar, P. (2017). Closed-loop controlling of boost converter is more efficient than open-loop controlling using MATLAB/Simulink. *Energy Procedia, 117*, 270–279. https://doi.org/10.1016/j.egypro.2017.05.131

[6]. Chen, Z., Zhang, Y., & Li, P. (2022). Wavelet-based feature extraction for fault detection in photovoltaic systems. *Journal of Energy Engineering*.

[7]. Kibria, A. N. M., & Ahmed, S. A. (2023). Advances in fault detection algorithms for PV systems. *Renewable Energy*.

[8]. Khan, N. A., Iqbal, M. T., & Nasir, M. (2015). Model predictive control-based multilevel inverter for solar water pumping system. *Proceedings of the 2015 IEEE 8th International Conference on Industrial and Information Systems (ICIIS)* (pp. 1–6). IEEE.

[9]. Kurukuru, V. S. B., Haque, A., Khan, M. A., Blaabjerg, F., & Davari, P. (2016). Constant power mode operation of photovoltaic (PV) arrays to ensure maximum power transfer capability of two-stage grid-connected PV systems. *IEEE Journal of Emerging and Selected Topics in Power Electronics, 4*(4), 1211–1227. https://doi.org/10.1109/JESTPE.2016.2615886

[10]. Raghuwanshi, R., & Gupta, V. (2015). Challenges in fault detection in transformerless PV systems. *Renewable Energy Journal*.

[11]. Rodriguez, F. J., & Wang, X. (2024). Machine learning-based classification for PV fault detection. *Journal of Electrical Engineering Research*.

[12]. Sakthivel, S., Arunachalam, V., & Jagatheesan, K. (2023). Detection, classification, and location of open-circuit and short-circuit faults in solar photovoltaic array: An approach using single sensor. *IEEE Journal of Photovoltaics*. https://doi.org/10.1109/JPHOTOV.2023.3304113

[13]. Villalva, M. G., Gazoli, J. R., & Filho, E. R. (2009). Comprehensive approach to modeling and simulation of photovoltaic arrays. *IEEE Transactions on Power Electronics, 24*(5), 1198–1208. https://doi.org/10.1109/TPEL.2009.2013862

[14]. Wang, X., & Rodriguez, F. J. (2024). Advances in transformerless PV fault detection using wavelet transform. *Journal of Electrical Systems*.

[15]. Xia, Z., Wang, Y., & Yang, L. (2021). Modelling of solar-powered three-phase induction motor pumping systems under fault conditions. *Renewable Energy Systems Journal*.